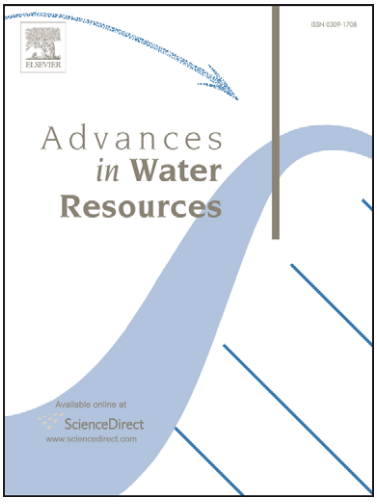

Critical and supercritical withdrawal from a two-layer fluid through a line sink in a partially bounded aquifer

Hong Zhang, Graeme C. Hocking, Brian Seymour

PII: S0309-1708(09)00140-7
DOI: 10.1016/j.advwatres.2009.09.002
Reference: ADWR 1462

To appear in: *Advances in Water Resources*

Received Date: 9 June 2009
Revised Date: 1 September 2009
Accepted Date: 2 September 2009

Please cite this article as: Zhang, H., Hocking, G.C., Seymour, B., Critical and supercritical withdrawal from a two-layer fluid through a line sink in a partially bounded aquifer, *Advances in Water Resources* (2009), doi: 10.1016/j.advwatres.2009.09.002

Critical and supercritical withdrawal from a two-layer fluid through a line sink in a partially bounded aquifer

Hong Zhang[1], Graeme C. Hocking[2] and Brian Seymour[3]

[1] Griffith School of Engineering, Griffith University, Australia
[2] Dept of Mathematics and Statistics, Murdoch University, Australia
[3] Dept of Mathematics, University of British Columbia, Canada

Abstract

The steady response of the interface between two fluids of different density in a bounded aquifer is considered during extraction through a line sink. Both critical and supercritical withdrawals are investigated. An analytical solution is developed to determine the interface location and withdrawal strength for critical withdrawals when only one fluid is pulled into the sink. Supercritical flows are considered in which both fluids are drawn directly into the sink. A boundary integral method is used to calculate the interface location that depends on the supercritical withdrawal rate and the aquifer configuration. It is shown that for each withdrawal rate greater than the critical value, the entry angle of the interface decreases as the withdrawal rate increases. The minimum entry angle depends on the aquifer configuration, i.e the ratio between the sink height and the impermeable boundary height. The steepest entry angle approaches $\frac{\pi}{2}$, where the interface shape approaches that given by the analytical solution for the critical rate, and the flow rate approaches the critical value. The viscosity ratio of the two fluids affects the effective withdrawal rate G. If the upper fluid is much more viscous than the lower fluid, coning is much less likely.

Keywords: critical withdrawal, supercritical withdrawal, hodograph method, boundary integral method, line sink

1. Introduction

There are a number of applications in which fluid is withdrawn from porous media. The most significant of these are undoubtedly oil/gas recovery and fresh water extraction from a salt stratified aquifer.

It is well known that withdrawal from several fluid layers of different density is marked by critical transitions from single to multi-layer flow as the outflow rate is increased. At low suction, buoyancy forces ensure that the total outflow comes from within the fluid layer adjacent to the outlet. If the flow is increased sufficiently, however, there is a "catastrophic" drawdown of the interface into the outlet resulting in the next fluid layer being pulled in. This critical transition, often termed "critical withdrawal", is of great practical importance since it affects the quality of the withdrawn fluid. The critical flow rate is defined as the maximum rate at which only the layer adjacent to the sink is withdrawn. At a higher "supercritical rate", fluid from both layers will be removed, which is often called coning.

This critical flow phenomenon was first studied by *Muskat and Wyckoff* [1935]. Other authors who have studied critical withdrawal using analytical methods for various aquifer configurations include *Bear and Dagan* [1964], *Gige*r [1989], *McCarthy* [1993], *Zhang and Hocking* [1997], *Zhang et al.* [1997] and recently, *Hocking and Zhang* [2008]. In this work the two fluids are assumed to be immiscible and the interface to be sharp.

However, limited research has been done for supercritical flow in porous media. *Yu* [1999] and *Henderson et al.* [2005] used a finite difference method to simulate an isothermal, monophasic, highly compressible flow in supercritical conditions, while *Hocking and Zhang* [2009] found various branches of solutions for supercritical withdrawal in an unbounded aquifer. The analogous problem of supercritical withdrawal in two-layer surface water bodies was considered by *Hocking* [1995], *Forbes* and *Hocking* [1998], and *Hocking* and *Forbes* [2001] using an integral equation approach to compute accurate numerical solutions.

In the present study, two homogeneous fluids separated by an infinitesimally thin interface near the withdrawal sink, and impermeable boundaries away from the sink, are considered. A line sink (a point in two dimensions) is located in the upper layer and withdraws fluid at some constant rate. An impermeable barrier exists separating the two layers at some distance from the sink. The physical plane is shown in Figure 1(a). The artificial device of using this impermeable barrier is equivalent to the "lateral edge drive" model of *McCarthy* [1993], and serves the purpose of maintaining horizontal flow within the two fluids at large distances from the sink. If this barrier were absent, the interface condition dictates that the elevation of the interface must be

unbounded. Unbounded flows can be considered by taking the limit as this barrier is moved away.

An analytical solution is developed for critical withdrawal, in which a cusp shaped interface is found to occur. At higher withdrawal rates, fluid from both layers will enter the sink after drawdown. Integral equations to be satisfied in both layers and equations matching the pressures across the interface are derived and solved numerically. A study of the effect of variations in several parameters is conducted, including viscosity and impermeable boundary location. In each case it is found that as the withdrawal rate increases, the interface near to the sink becomes flatter, eventually reaching a point where it can no longer maintain a concave shape, a point beyond which solutions can no longer be obtained. As the withdrawal rate decreases, the solutions approach the critical flow solutions.

2. Theoretical Formulation

2.1 Problem Set-up

Consider a homogeneous, isotropic, porous medium with intrinsic permeability κ, where the fluids are separated by an interface of infinitesimal thickness into two homogeneous regions of different density with impermeable boundaries as seen in Figure 1(a). The fluids located below and above the impermeable boundary (IL) are defined as *fluid 1* and *fluid 2*, with densities ρ_1 and ρ_2 respectively. A line sink (S) is located at a distance H above the impermeable boundary. The horizontal distance between the sink and each impermeable boundary (L) is x_L. The point at infinity along the impermeable boundary is I. The sink extracts a total flux Q per unit time, per unit width.

Using complex variables, let the physical plane correspond to the Z-plane shown in Figure 1(a), where $z = x+iy$. The origin is located directly below the sink at the level of the solid boundaries, with $y=\eta(x)$ as the equation of the interface. The velocity potentials in each region in two-dimensional steady flow satisfy Darcy's Law [*Strack*, 1989]:

$$\begin{cases} \Phi_1 = \dfrac{\kappa}{\mu_1}(p+\rho_1 g y)+C_1 \\ \Phi_2 = \dfrac{\kappa}{\mu_2}(p+\rho_2 g y)+C_2 \end{cases}, \qquad (1)$$

where κ is the intrinsic permeability; μ_1 and μ_2 are the dynamic viscosities of the fluids; p is the pressure at the location of y; C_1 and C_2 are constants. Matching the pressure across the interface between the two regions gives the condition on the interface, $y = \eta(x)$, that

$$\frac{d\Phi_1}{ds} - \gamma \frac{d\Phi_2}{ds} = K \frac{dy}{ds}, \tag{2}$$

where $\gamma = \frac{\mu_2}{\mu_1}$, $K = \frac{\kappa g(\rho_1 - \rho_2)}{\mu_1}$ and s is the arc length along the interface. When the withdrawal rate is less than critical, the lower fluid is stationary and the entire stationary fluid region is assumed to be at a constant potential. It is noted that since the potential due to the sink is logarithmic, then if only one fluid is flowing the condition on the interface leads to an interface of unbounded elevation as x approaches infinity. However, in the fully two-layer flow, we require that $\mu_1\Phi_1$ approaches $\mu_2\Phi_2$ on the interface as x approaches infinity.

2.2 Analytical solution for critical withdrawal

Critical withdrawal is the situation in which a small increase in discharge above the current withdrawal rate will cause the denser fluid to enter the outlet directly. When the withdrawal rate is lower than the critical value the denser fluid is stationary and can be assumed to be at a constant potential. As the location of the interface is unknown it is difficult to obtain an exact solution for the supercritical flow case. However, in the critical case, a hodograph method, similar to that of *Bear and Dagan* [1964] can be employed.

For critical withdrawal, there exists a cusp point, C, as shown in Figure 1(a). The vertical distance between C and the horizontal impermeable boundary is h_c. Let $\alpha = \Phi(x, y) + i\Psi(x, y)$ be the complex potential, and $W = u(x, y) - iv(x, y)$ be the complex velocity, then $W = -\frac{d\alpha}{dz}$. The flow region can be mapped on the hodograph α-plane and W-plane as shown in Figures 1(b) and 1(c). Using an inverse transformation $V = \frac{K}{W}$, the flow region can be transformed to the V-plane as shown

in Figure 1(d). Then, using a Schwartz-Christoffel mapping, $\frac{dV}{d\zeta} = A\zeta^{-\frac{3}{2}}\frac{\zeta - a}{\zeta + 1}$, the flow region in both the *V*- and ωplanes are mapped to the upper half of the ζplane by

$$\omega = \frac{Q}{\pi}(\ln\frac{\zeta - b}{\zeta}),$$
$$V = \frac{2i}{\pi}\left(\tanh^{-1}\left(\sqrt{\zeta}\right) + \frac{a}{(1+a)}\frac{1}{\sqrt{\zeta}}\right), \tag{3}$$

where *a* and *b* are mapping parameters as shown in Figure 1. Therefore the entire boundary can be computed by integrating

$$\frac{dz}{d\zeta} = -\frac{2i}{\pi}\left(\tanh^{-1}\left(\sqrt{\zeta}\right) + \frac{a}{1+a}\frac{1}{\sqrt{\zeta}}\right)\left(\frac{1}{\zeta - b} - \frac{1}{\zeta}\right) \tag{4}$$

along the real ζaxis. We note that in Figure 1(e), $V(b) = 0$ and hence the parameter *a,* (*-1<a<0*), in the transformation in (3) can be determined by solving $a = -\frac{\tanh^{-1}\sqrt{b}}{\tanh^{-1}\sqrt{b} + 1/\sqrt{b}}$. Using the non-dimensionalisation $z^* = z/H$, $\omega^* = \omega/\frac{Q}{\pi}$, z^* can be expressed in terms of ζ and the shape of the interface determined as

$$x^*(\zeta) = x_L^* - G_{cr}\int_{-1}^{\zeta}\frac{b}{\zeta(\zeta - b)}\left[\frac{1}{\pi}\ln\frac{\sqrt{-\zeta}+1}{\sqrt{-\zeta}-1} + \frac{2a}{(1+a)\pi}\frac{1}{\sqrt{-\zeta}}\right]d\zeta,$$
$$y^*(\zeta) = -G_{cr}\ln\frac{\zeta - b}{(1+b)\zeta}. \tag{5}$$

for $-\infty < \zeta < -1$ and $G_{cr} = \frac{Q_{cr}}{\pi KH}$. As $\zeta \to -\infty$, then $h_c = y^*(-\infty) \to G_{cr}\ln(1+b)$. The distance between the cusp point and the sink can be calculated by integrating Equation (4) for $b \le \zeta < \infty$. Therefore, the critical withdrawal rate can be determined as

$$G_{cr} = \frac{1}{\ln(1+b) + \frac{2}{\pi}\int_b^{\infty}\frac{b}{\zeta(\zeta+b)}\left[\tanh^{-1}\sqrt{\zeta} - \frac{\sqrt{b}\tanh^{-1}\sqrt{b}}{\sqrt{\zeta}}\right]d\zeta}. \tag{6}$$

It can be seen from Equations (5) and (6) that both the impermeable location x_L^* and the critical withdrawal rate vary with the parameter *b*.

A small increase in the withdrawal rate above the critical value, G_{cr}, will cause the fluid from the lower layer to enter the sink, leading to supercritical withdrawal, i.e. both fluids will enter the sink. In order to find solutions for this case, we need to use

a numerical scheme such as the boundary integral method proposed below, as the hodograph method is no longer applicable.

2.3 Boundary integral method for supercritical withdrawal

For supercritical rates, we seek solutions in which the interface is drawn up a distance H to a point where it enters the sink with an angle α to the horizontal, as shown in Figure 1(a). The analytic solution cannot be found for the supercritical case. Since the flux from each layer (see below) depends on the angle of entry, α then in the right half-plane the flux from the lower fluid is $Q\left(\frac{\pi}{2}-\alpha\right)/\pi$ and from the upper fluid it is $Q\left(\frac{\pi}{2}+\alpha\right)/\pi$. Fluid is withdrawn from both above and below the interface. The velocity potentials of the separate flow fields below and above the interface must satisfy Laplace's equation,

$$\begin{cases} \nabla^2\Phi_1(x,y)=0, \quad y<\eta(x), \\ \nabla^2\Phi_2(x,y)=0, \quad y>\eta(x). \end{cases} \tag{7}$$

As the sink is approached, the velocity potentials must have the correct behaviour,

$$\begin{cases} \Phi_1 \to \dfrac{Q_1}{\frac{\pi}{2}-\alpha}\ln\sqrt{x^2+(y-H)^2} \;\; as \;\; (x,y)\to(0,H), \; y<\eta(x), \\ \Phi_2 \to \dfrac{Q_2}{\frac{\pi}{2}+\alpha}\ln\sqrt{x^2+(y-H)^2}, \; as \;\; (x,y)\to(0,H), \; y>\eta(x), \end{cases} \tag{8}$$

where Q_1 and Q_2 are the respective total dimensional fluxes per unit width (from the right half-plane) from within the two regions. There is a relationship between these two values that must hold if the dynamic condition on the interface is to be satisfied. Applying Darcy's Law (*Bear* [1972]) to the streamline along the interface, and noting that for steady flow there must be no pressure difference across the interface leads to Equation (2).

Considering the behaviour of the flow near the sink (8) and the interface condition (2), if the flow into the line sink is radial, then there is

$$\frac{\gamma Q_2}{2r_d\left(\frac{\pi}{2}+\alpha\right)}-\frac{Q_1}{2r_d\left(\frac{\pi}{2}-\alpha\right)}=K\sin\alpha, \tag{9}$$

where r_d is the radius of the outlet. As $r_d \to 0$, it follows that

$$\frac{Q_1}{\frac{\pi}{2}-\alpha} = \gamma \frac{Q_2}{\frac{\pi}{2}+\alpha}, \text{ and } Q = Q_1 + Q_2. \tag{10}$$

Defining the following dimensionless variables,

$$y^* = y/H,\ x^* = x/H,\ \Phi_1^* = \Phi_1 / \frac{Q_1}{\frac{\pi}{2}-\alpha},\ \Phi_2^* = \Phi_2 / \frac{\gamma Q_2}{\frac{\pi}{2}+\alpha},$$

the non-dimensional form of the dynamic interface condition becomes

$$\frac{d\eta^*}{ds} = \frac{2\gamma\pi}{\pi(1+\gamma)+2\alpha(1-\gamma)} G\left(\frac{d\Phi_1^*}{ds} - \frac{d\Phi_2^*}{ds}\right), \text{ and } G = \frac{Q}{\pi KH} \tag{11}$$

with

$$\begin{aligned} &\Phi_1^* \to \ln\left[x^{*2} + (y^*-1)^2\right]^{\frac{1}{2}}, \text{ as } (x^*, y^*) \to (0,1),\ y^* < \eta^*(x^*), \\ &\Phi_2^* \to \ln\left[x^{*2} + (y^*-1)^2\right]^{\frac{1}{2}}, \text{ as } (x^*, y^*) \to (0,1),\ y^* < \eta^*(x^*). \end{aligned} \tag{12}$$

The asterisks denote dimensionless variables and will be dropped for simplicity. G is therefore a measure of the flow strength. Another condition to be satisfied is that there be no flow across the interface. This condition can be ensured by enforcing the condition $\Psi_1 = \Psi_2 = 0$ on the stream functions along the interface. We define a complex potential for each region that builds in the correct behaviour both near the sink and in the far field, and then compute the corrections to these. Options that satisfy these requirements are

$$\begin{cases} f_1 = \Phi_1 + i\Psi_1 = \ln(z-i) - \dfrac{2\alpha}{\pi}\ln(z - i\dfrac{\pi}{2\alpha}) + w_1, & y < \eta(x), \\ f_2 = \Phi_2 + i\Psi_2 = \ln(z-i) + \dfrac{2\alpha}{\pi}\ln(z + i\dfrac{\pi}{2\alpha}) + w_2, & y > \eta(x), \end{cases} \tag{13}$$

where α is the angle of the interface at the point of entry into the sink and $w_j = \phi_j + i\psi_j$, $j=1, 2$, are the correction terms for the full velocity potential. In each layer, they represent the addition of another singular point outside the domain of interest. These are a line sink at $y = \frac{\pi}{2\alpha}$ for the lower fluid and a line source at $y = -\frac{\pi}{2\alpha}$ for the upper fluid. These choices satisfy the requirement that the line given by $\Psi_j = 0,\ j = 1,2$ enters the sink at an angle α to the horizontal provided

$$\begin{cases} \psi_1(x,\eta) = -\arctan\left(\dfrac{\eta(x)-1}{x}\right) - \dfrac{2\alpha}{\pi}\arctan\left(\dfrac{\eta(x)-\pi/2\alpha}{x}\right), \\ \psi_2(x,\eta) = -\arctan\left(\dfrac{\eta(x)-1}{x}\right) + \dfrac{2\alpha}{\pi}\arctan\left(\dfrac{\eta(x)+\pi/2\alpha}{x}\right), \end{cases} \tag{14}$$

The choice of f_1 and f_2 also ensures that $w_j \to 0,\ \mathrm{j}=1,2$ as $|z| \to \infty$ or as $z \to i$. The functions

$$\begin{cases} w_1 = \phi_1 + i\psi_1, & y < \eta(x), \\ w_2 = \phi_2 + i\psi_2, & y > \eta(x), \end{cases} \tag{15}$$

must be analytic in their respective domains. Following *Forbes* [1985] and *Hocking* [1995], and applying Cauchy's Theorem to $w_j - 0,\ j=1,2$, on both regions, we obtain

$$\pi\, w_j(z_0) = \int_{\Gamma_j} \frac{w_j(z)}{z-z_0}dz,\ j=1,2 \quad ,$$

where $\Gamma_j - 0,\ j=1,2$ are the contours shown in Figure 1(f), and z_0 lies on the boundary in each case. Now, since $w_j \to 0,\ j=1,2$ as $|\mathrm{z}| \to \infty$, the contribution of that part of w_j that consists of the circular arc can be shown to be zero. Thus we only need to integrate along the interface. Using an arc length variable, *s,* along the interface starting from the sink, then

$$\left(\frac{dx}{ds}\right)^2 + \left(\frac{d\eta}{ds}\right)^2 = 1, \tag{16}$$

and using the chain rule we can write

$$\pi\, i\, w_1(z(s)) = \int_{-\infty}^{\infty} \frac{w_1(z(t))\,dz/dt}{z(t)-z(s)}dt,\ -\pi\, i\, w_2(z(s)) = \int_{-\infty}^{\infty} \frac{w_2(z(t))\,dz/dt}{z(t)-z(s)}dt, \tag{17}$$

where s and t are both arc lengths, but s defines a particular location and t is the variable of integration. Since ψ_1, ψ_2 are known along the interface from equation (14), these represent integral equations for ϕ_1 and ϕ_2 respectively. Taking the real parts and utilizing the symmetry of the situation about the line $x=0$, i.e.

$$\begin{cases} x(-s) = -x(s),\ y(-s) = y(s),\ x'(-s) = x'(s),\ y'(-s) = -y'(s), \\ \phi_j(-s) = \phi_j(s), \psi_j(-s) = -\psi_j(s),\ j=1,2, \end{cases} \tag{18}$$

the integral equations become

$$\phi_j(s) = \frac{\kappa_j}{\pi}\int_0^\infty \phi_j(t)\left(\frac{-x'(t)\Delta y + y'(t)\Delta x}{\Delta x^2 + \Delta y^2} - \frac{x'(t)\Delta y - y'(t)\Delta x_+}{\Delta x_+^{\,2} + \Delta y^2}\right) + \psi_j(t)\left(\frac{x'(t)\Delta x + y'(t)\Delta y}{\Delta x^2 + \Delta y^2} + \frac{x'(t)\Delta x_+ + y'(t)\Delta y}{\Delta x_+^{\,2} + \Delta y^2}\right)dt, \quad j = 1, 2, \tag{19}$$

where $\Delta x = x(t) - x(s)$, $\Delta x_+ = x(t) + x(s)$ and $\Delta y = y(t) - y(s)$, and $\kappa_1 = 1, \kappa_2 = -1$. The problem to be solved is the combination of the two integral equations given by (19) and the interface condition (11).

This system must be solved numerically. The logarithmic singularity near the sink must be treated carefully to avoid numerical problems, but the following method was successful:

1. For the nonlinear integral equations (19), the domain $[0, \propto)$ of the independent variable s was truncated to a finite point, $z_T = (x_T, 0)$, along the impermeable boundary, and the interval was discretised into the set of points s_j, $j = 1, 2, 3, \ldots N_i, \ldots N$. There are N_i points on the interface and (N- N_i) points on the impermeable boundary. The exact location of these points was usually uniform, but in some cases a quadratic distribution was used to crowd many points close to the region of greatest change near to the sink. An initial guess was made for the unknown values of the correction term of velocity potential ϕ_1 and ϕ_2, the derivative of the interface location $\eta'(s)$ and the entry angle of the interface into the sink, α A fixed value of G was given.
2. The other variables, $x(s)$ and $y(s)$ were computed by finding $x'(s)$ from (15) and then using numerical integration.
3. Using $x, \eta, x'(s), \eta'(s), \phi_1, \phi_2$ along the interface, the error in (17) was computed and a damped Newton iteration scheme was applied.
4. Once ϕ_1, ϕ_2 had been obtained, a forward difference scheme was used to calculate their derivatives and the error in the interface condition (12) was evaluated. If the error is small at all points on the interface, say less than 10^{-9}, the algorithm was stopped. Otherwise, Newton's method was used to update $\eta'(s)$, and repeat from step 2.

The accuracy of the numerical integration is crucial to the solution of the full problem. The singular part of the principal-value integral in (19) was removed by noting that

$$\int_0^{z_T} \frac{w_j(z)}{z-z_0}dz = \int_0^{z_T} \frac{w_j(z)-w_j(z_0)}{z-z_0}dz + w_j(z_0)\ln\left(\frac{z_T-z_0}{z_0}\right),$$

where z_T corresponds to the point at which the integral is truncated. It is also essential to include an approximation to the portion of the integral that is neglected. Both ϕ and ψ can be shown to behave like $O(s^{-1})$ as $s \to \infty$, so a simple correction term can be added to each integral to account for the truncation. For the same impermeable boundary location, various grid points were tested for convergence. The iteration scheme converged in only 4 or 5 iterations and solutions to graphical accuracy were found with N as small as $N=80$, but most solutions were computed with $N=200$. i.e. with *200* collocation points on the interface.

3 Results and Discussion

3.1 Critical withdrawal

The interface locations were calculated for the critical cases as described in Section 2.1. Figure 2 shows examples of the interface computed in this way. In the analytical solution described in Section 2.1, the parameters a and b determine the location of the impermeable boundary x_L. When $b \to \infty, a \to -1$, then $x_L \to \infty$, i.e., the impermeable boundary goes to infinity, and when $b \to 0, a \to 0$, then $x_L \to 0$, i.e., the impermeable boundary moves to directly beneath the sink (see Figure 3). Figures 4 and 5 further demonstrate the relationship between h_c and G_{cr} with x_L. It can been seen that as x_L goes to infinity, i.e., the layer is unbounded, the cusp point moves toward the sink but G_{cr} approaches a finite value close to G_{cr} = 0.06; while when x_L goes to 0, the cusp point moves towards the impermeable boundary, i.e. two fluids are separated by the impermeable boundary completely, and G_{cr} goes to infinity. These findings are in agreement with the results of *Bear and Dagan* [1964] for upconing toward a line sink in an unbounded aquifer, and *Zhang et al.* [1997] for a vertically bounded aquifer.

3.2 Supercritical withdrawal

A series of simulations was performed using the boundary integral method discussed in Section 2.3 to compare with the hodograph solutions. The value of the viscosity ratio was kept at γ=1 initially. The interface locations at the lowest supercritical

withdrawal parameter G values were compared with the critical case for two finite boundary locations x_L as shown in Figure 6. As expected, there is a good agreement between the two cases. It was found that there was a range of values of G for which solutions existed for each x_L. If a supercritical G slightly greater than the critical rate was specified, the entry angle of the interface was very close to $\frac{\pi}{2}$. As the value of G was increased, the magnitude of the entry angle of the interface into the sink decreased and eventually the method failed when the entry angle was slightly greater than $\alpha = \arctan\left(\frac{1}{x_L}\right)$. This value corresponds to that at which the interface can no longer maintain a concave shape. Figure 7 shows an example of the interface shapes for the case $x_L=20$. At the lowest value of $G=0.1059$, the entry angle equals 1.55 and the interface solution is close to the critical single-layer flow, while at the highest, it is close to being a straight line from the sink to the impermeable barrier. A large increase in G is required to get solutions at low entry angle, α for this configuration.

Figure 8 demonstrates the range of the supercritical withdrawal rate and its corresponding entry angle for various impermeable boundary locations. As the impermeable boundary moves further away from the sink, the lowest G decreases from 0.33 to 0.14 and then to 0.1 for x_L = 5, 10 and 20, which correspond to their critical rates (as shown in Figure 4). However, Figure 8 also shows that the entry angle asymptotes to the horizontal as G increases. With the impermeable boundary moving further away from the sink, the entry angle is highly correlated to the ratio $\frac{h_c}{x_L}$.

The influence of the viscosity ratio on the interface was also examined. Figure 9 shows interface profiles with various viscosity ratios for $x_L=20$ and $G=1$. When $\gamma << 1$, i.e. *fluid 1* in the upper layer is much more viscous than *fluid 2* in the lower layer, the effective withdrawal rate is reduced compared to $\gamma \approx 1$, as can be deduced from equation (11) by noting that γG could be used as a single parameter. When $\gamma >> 1$, i.e. *fluid 1* in the upper layer is much less viscous than *fluid 2* in the lower layer, the effective withdrawal rate is increased, but depends less on the viscosity ratio, as can be seen in Figure 10; the interface entry angle changes little when

$\gamma >> 1$. This suggests that if the upper fluid is much more viscous than the lower fluid, coning is much less likely.

4 Conclusions

The critical and supercritical withdrawals through a line sink of two fluids of different density and viscosity in an isotropic, homogeneous two-dimensional bounded aquifer are investigated. An analytical solution is developed to find the interface location for critical withdrawal using a hodograph method, and a boundary integral method is used to compute the interface shapes for the supercritical case in which both fluids are drawn directly into the sink. Based on the analytical and numerical results presented, the following conclusion can be drawn:

1. For critical withdrawal a cusp-shaped interface can be calculated at a unique value of the non-dimensional flow rate for a fixed impermeable boundary location. As the location of the impermeable boundary is moved outward, the cusp moves upward toward the sink and the interface tends to negative infinity. The critical value of G approaches 0.06 in this limit.
2. For supercritical withdrawal rates, the interface shape for the minimal rate is essentially the same as that for the critical case solved by the hodograph method; and the entry angle of the interface approaches $\frac{\pi}{2}$. In the limit as the impermeable boundary moves away while being kept at a fixed, finite vertical elevation, we obtain solutions for a range of withdrawal rates above the critical value. As the value of G increases, the magnitude of the entry angle decreases. The minimum entry angle depends on the ratio between the sink height and the impermeable boundary location. Solutions can not be obtained in which the interface is not concave, leading to a limiting entry angle and value of G for each aquifer configuration. Further work is required to understand the influence of impermeable boundaries at different locations in the flow domain.
3. The viscosity ratio of the two fluids affects the effective withdrawal rate G. When *fluid 1* in the upper layer is much more viscous than *fluid 2* in the lower layer, the effective withdrawal rate is reduced to γG. On the other hand, when *fluid 1* in the upper layer is much less viscous than *fluid 2* in the lower layer,

viscosity differences have a relatively minor effect on the effective withdrawal rate.

Notation

H	vertical distance between the sink and the impermeable boundary, [L]
$\rho_{1,2}$	density of fluid, [ML^{-3}]
κ	intrinsic permeability, [L^2]
μ	dynamic viscosity of the fluid, [$MS^{-1}L^{-1}$]
p	fluid pressure, [$ML^{-1}T^{-2}$]
$\Phi_{1,2}$	velocity potential, [L]
$Q_{1,2}$	pumping rate per unit width, [L^2T^{-1}]
x	horizontal location, [L]
y	vertical location, [L]
u	horizontal velocity, [LT^{-1}]
v	vertical velocity, [LT^{-1}]
U_m	maximum velocity along the impermeable boundary, [LT^{-1}]
η	interface location, [L]
α	angle between interface and horizontal, [Rad]
K	non-dimensional hydraulic conductivity
G	non-dimensional pumping rate
ω	complex potential
W	complex velocity
*	superscript indicating a dimensionless variable
$_{1,2}$	subscript indication the fluid in lower and upper layers respectively

Reference

Bear, J (1972) *Dynamics of Fluids in Porous Media*, McGraw Hill.

Bear, J and Dagan, G (1964) Some exact solutions of interface problems by means of the hodograph method. *J. Geophys. Res.*, **69**, 8, 1563-1572.

Giger, FM (1989) Analytic 2-D models of water cresting before breakthrough for horizontal wells. *SPE Res. Engineering*, November, pp 409-416.

Forbes, LK (1985) On the effects of non-linearity in free-surface flow about a submerged point vortex. *J. Engng Math* **19**, 139-155.

Forbes, LK and Hocking, GC (1998) Withdrawal from a two-layer inviscid fluid in a duct. *J. Fluid Mech.*, **361**, 275-296.

Henderson, N, Flores, E, Sampaio, M, Freitas, L and Platt, GM (2005) Supercritical fluid flow in porous media: modeling and simulation. *Chemical Engineering Science*, 60, 1797 – 1808.

Hocking, GC (1995). Supercritical withdrawal from a two-layer fluid through a line sink. *J. Fluid Mech.*, **297**, 37-47.

Hocking, GC and Forbes, LK (2001) Supercritical withdrawal from a two-layer fluid through a line sink if the lower layer is of finite depth. *J. Fluid Mech.*, **428**, 333-348.

Hocking, GC and Zhang, H (2009) Coning during withdrawal from two fluids of different density in a porous medium. *Journal of Engineering Mathematics*, DOI 10.1007/s10665-009-9267-1.

Hocking, GC and Zhang, H (2008) A Note On Withdrawal From A Two-Layer Fluid Through A Line Sink In A Porous Medium, *The ANZIAM Journal*, Volume 50 Issue 01, 101-110, doi:10.1017/S144618110800028X.

McCarthy, JF (1993) Gas and water cresting towards horizontal wells. *J. Aust. Math. Soc.*, Ser. B, 35, 174-197.

Muskat M, Wyckoff RD (1935) An approximate theory of water coning in oil production. *American Institute of Mining Engineers, Petroleum Development Technologies*, vol. 114, 144–163.

Strack, ODL. (1989) Groundwater Mechanics. Prentice Hall.

Yu D, Jackson K, Harmon TC (1999) Dispersion and diffusion in porous media under supercritical conditions. *Chemical Engineering Science,* 54, 357.

Zhang H, Hocking GC and Barry, DA (1997) An analytical solution for critical withdrawal of layered fluid through a line sink in a porous medium. *J. Austral. Math. Soc. Ser. B*, 39, 271-279.

Zhang, H. and Hocking, GC (1997) Axisymmetric flow in an oil reservoir of finite depth caused by a point sink above an oil-water interface. *J. Eng. Math.*, 32(4), 365-376.

List of figures:

Figure 1: (a) The domain configuration. (b) ω-plane. (c) W-plane. (d) V-plane. (e) Lower half of ζ-plane. (f) Contours used in the derivation of the integral equation (17).

Figure 2: The interface locations at critical conditions with various x_L = 6 (dashed line), x_L = 20 (dotted line) and x_L = 50 (solid line).

Figure 3: The relationship between the location of the impermeable boundary and the parameters a and b in the analytic solutions.

Figure 4: The relationship between the location of the impermeable boundary and the critical withdrawal rate.

Figure 5: The relationship between the location of the impermeable boundary and the cusp point elevation.

Figure 6: Interface shape comparison between the critical flow and the minimum supercritical cases: (a) $x_L=20$. (b) $x_L=10$.

Figure 7: Interface shapes for various G when $x_L=20$. The maximum and minimum G values are 4.2 and 0.09, respectively. The minimum value is close to critical.

Figure 8: The supercritical withdrawal rate and the corresponding entry angle for several impermeable boundary locations.

Figure 9: Interface profiles with various viscosity ratios for $x_L=20$ and $G=1$.

Figure 10: The effect of the viscosity ratio on the entry angle of the interface for $x_L=20$ and $G=1$.

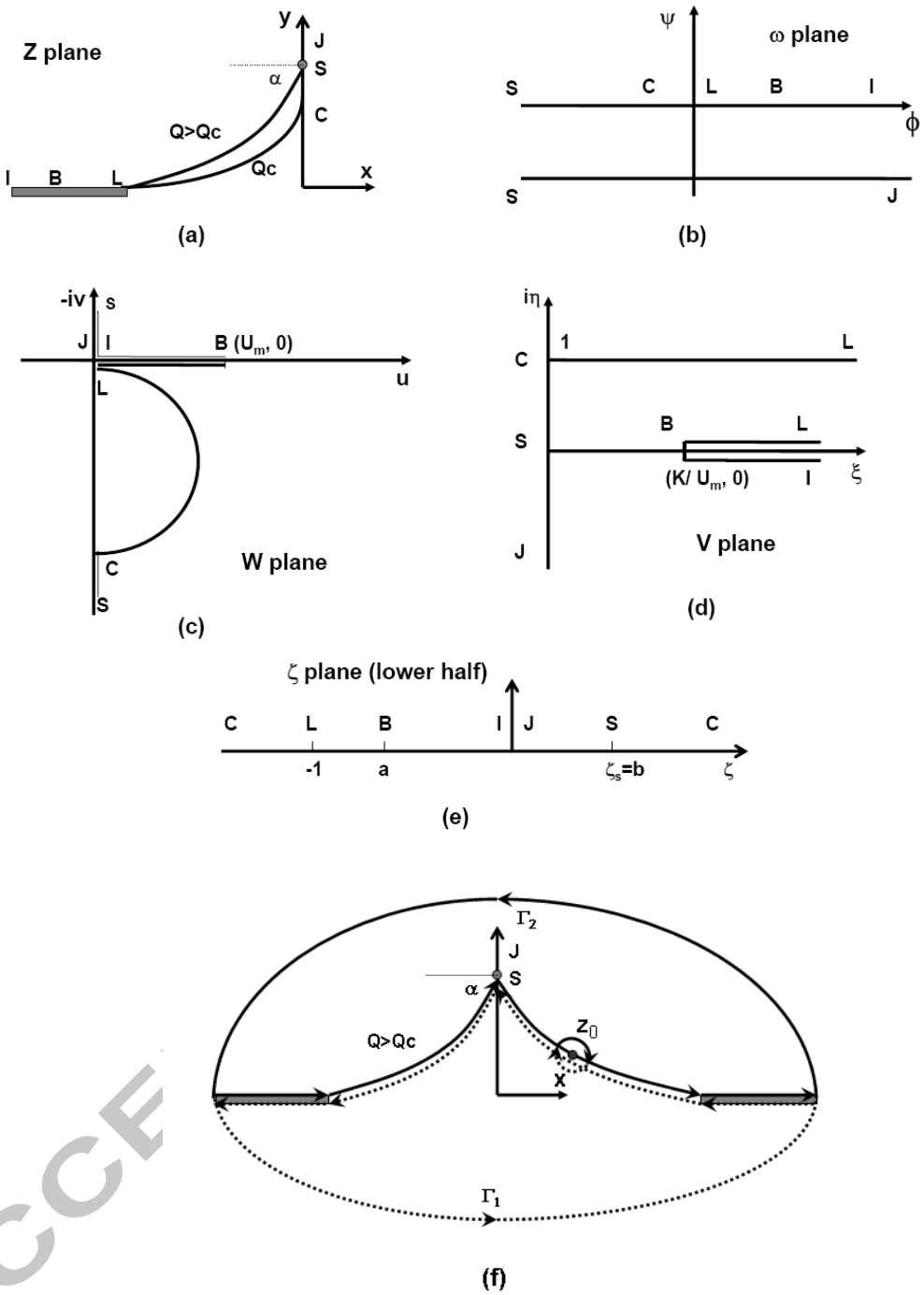

Figure 1: (a) The domain configuration. (b) ωplane. (c) W-plane. (d) V-plane. (e) Lower half of ζplane. (f) Contours used in the derivation of the integral equation (17).

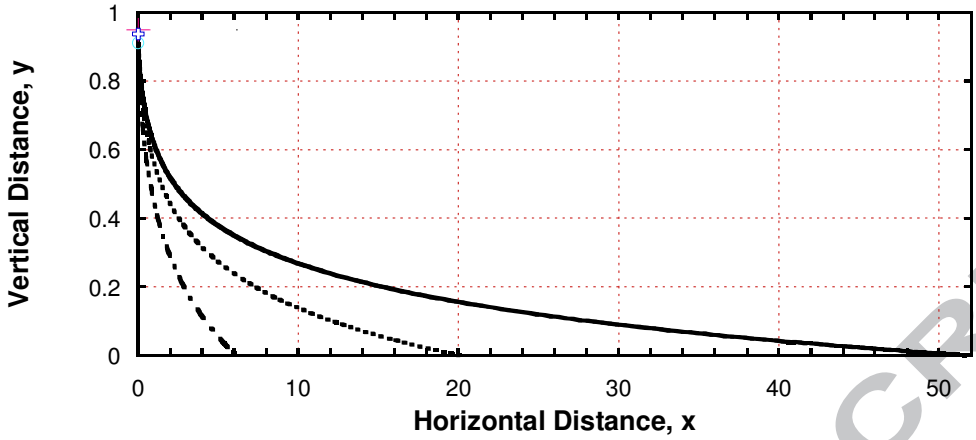

Figure 2: The interface locations at critical conditions with various x_L = 6 (dashed line), x_L = 20 (dotted line) and x_L = 50 (solid line).

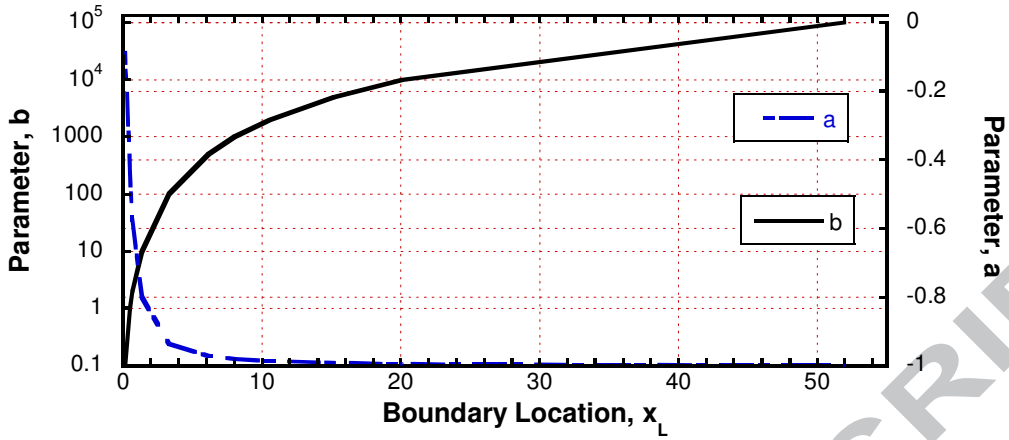

Figure 3: The relationship between the location of impermeable boundary and the parameters *a* and *b* in analytic solutions.

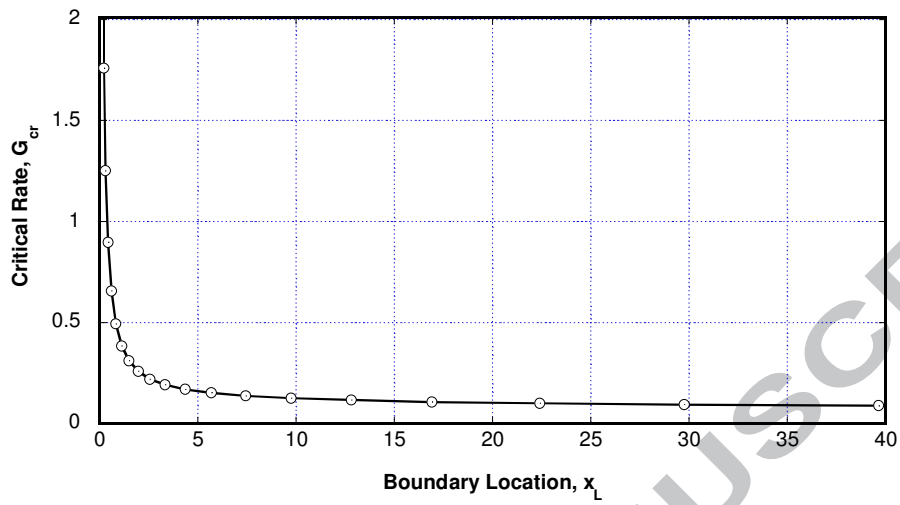

Figure 4: The relationship between the location of impermeable boundary and the critical withdrawal rate.

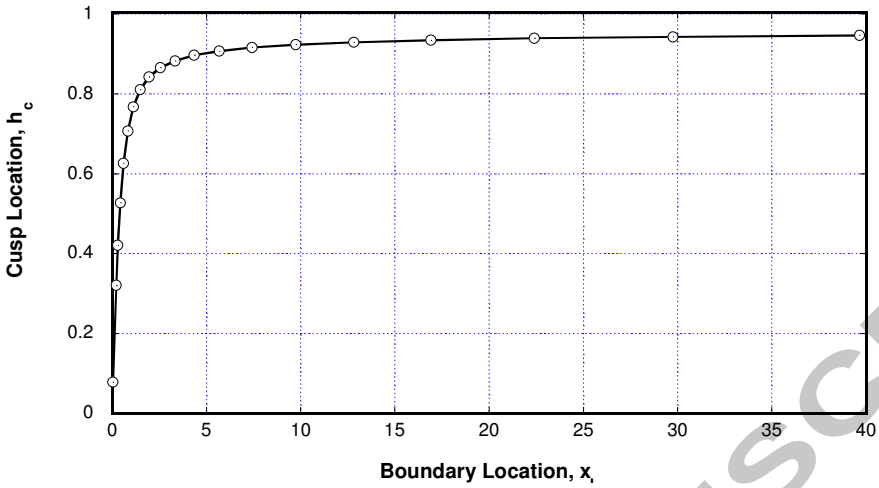

Figure 5: The relationship between the location of impermeable boundary and the cusp point location.

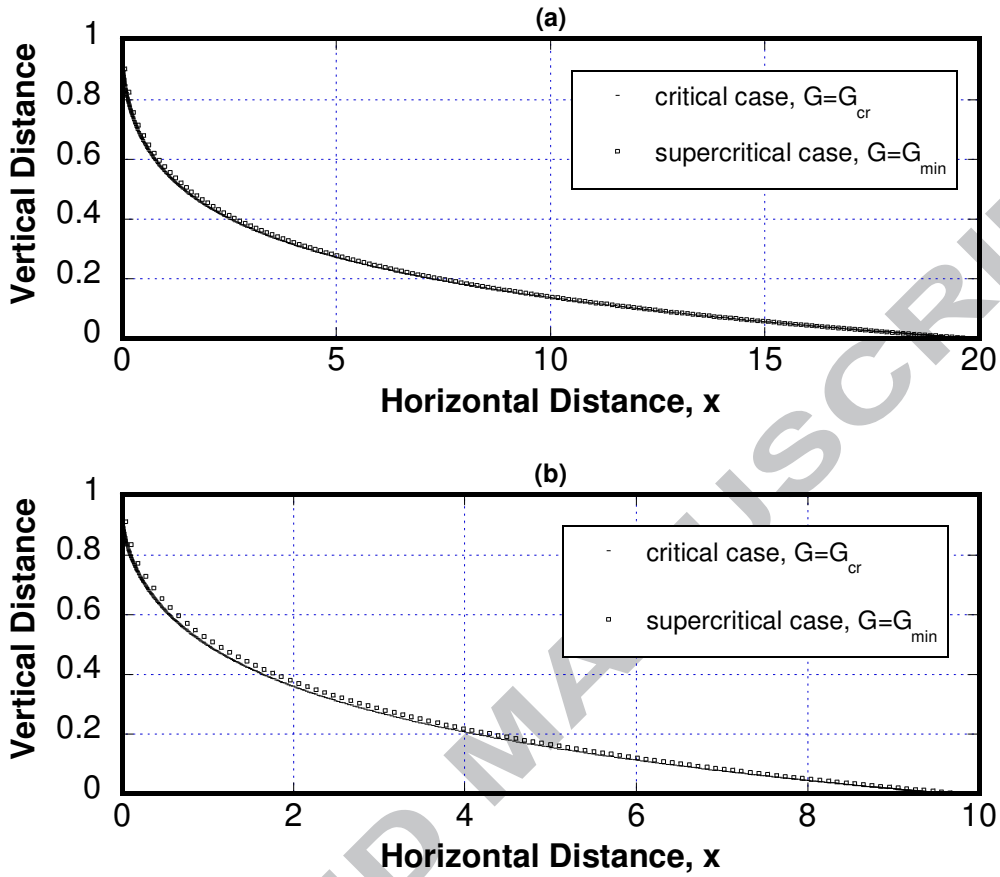

Figure 6: Interface locations comparison between critical and minimum supercritical cases: (a) $x_L=20$. (b) $x_L=10$.

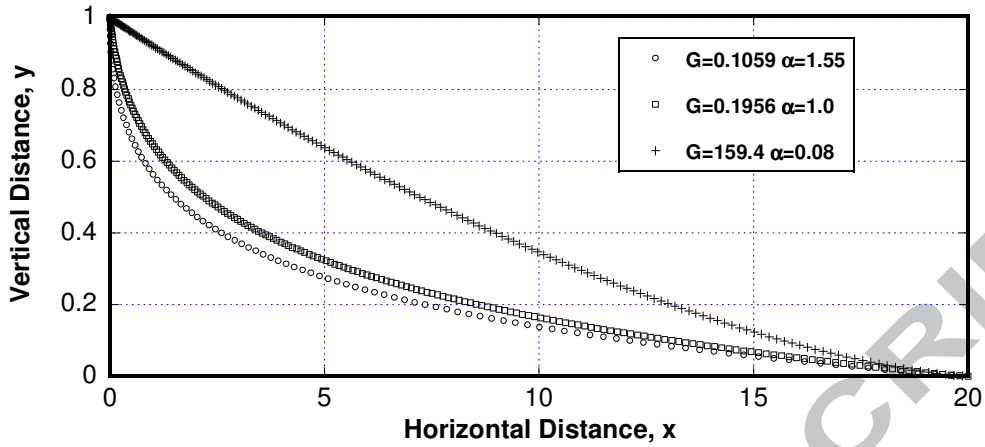

Figure 7: Interface locations for various G when $x_L=20$, where maximum and minimum G are 159.4 and 0.1059, respectively. The minimum value is close to critical.

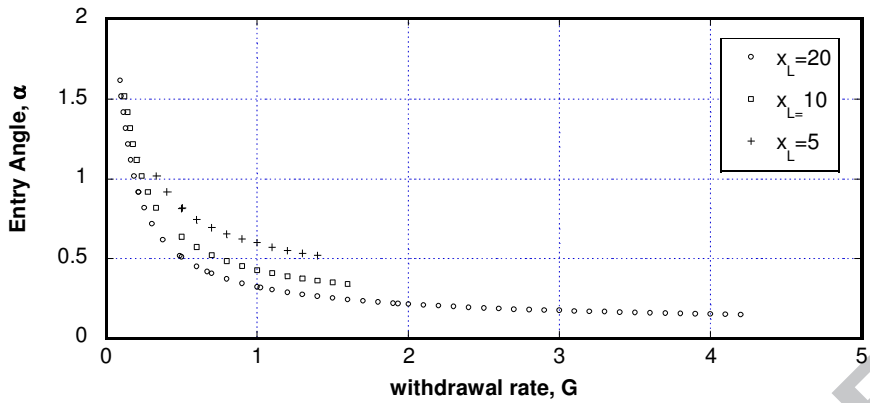

Figure 8: The range of the supercritical withdrawal rate and its corresponding entry angle for various impermeable boundary locations.

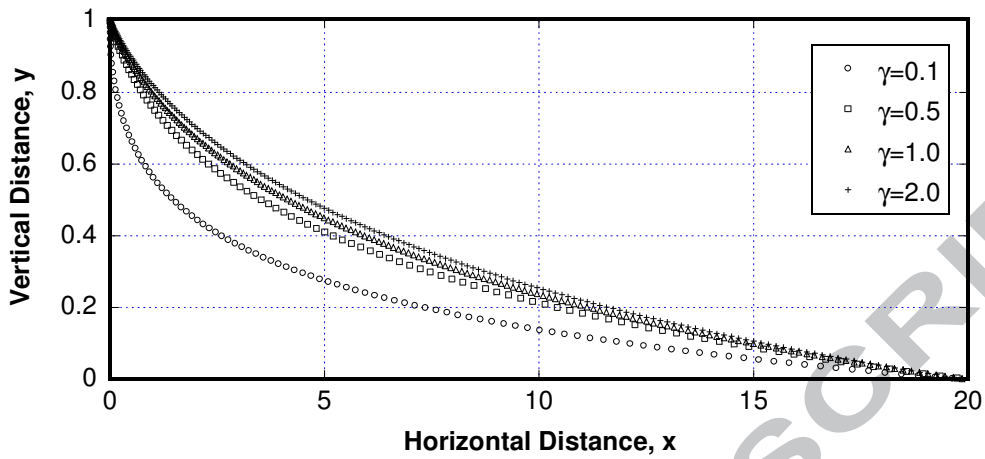

Figure 9: Interface profiles with various viscosity ratios for $x_L=20$ and $G=1$.

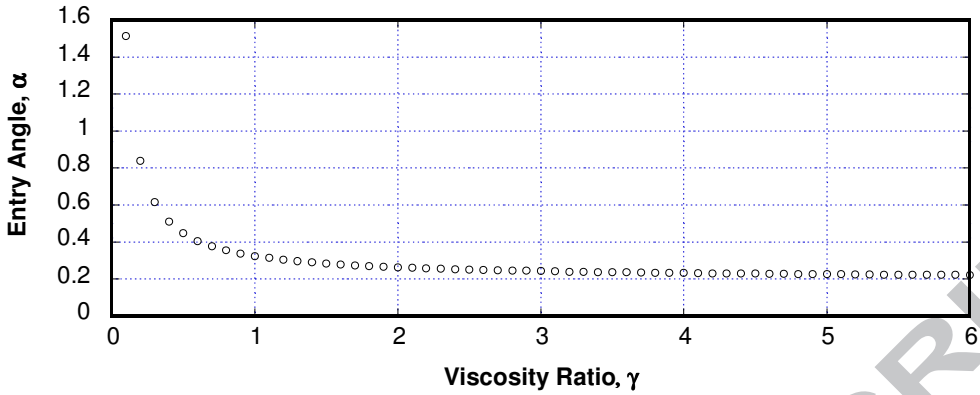

Figure 10: The effect of the viscosity ratio on the entry angle of the interface for xL=20 and G=1.